AASERT Grant #N00014-93-1-0827

Second Semi-Annual Progress Report
(covering the period of 01/16/94-07/15/94)

Project Title: Investigation of a Normal Incidence High-Performance P-type Strained Layer $In_{0.3}Ga_{0.7}As/In_{0.52}Al_{0.48}As$ Quantum Well Infrared Photodetector.

Submitted to

Max N. Yoder

Office of Naval Research
Code 3140
800 North Quincy Street
Arlington, VA 22217-5000

Prepared by

Jerome T. Chu
Student

and

Sheng S. Li
Professor

Department of Electrical Engineering
University of Florida
Gainesville, FL 32611

Tel. (904) 392-4937
Fax (904) 392-8671
E-mail: ShengLi@ENG.UFL.EDU

July 15, 1994

REPORT DOCUMENTATION PAGE

Form Approved
OMB No. 0704-0188

1. AGENCY USE ONLY (Leave blank)	2. REPORT DATE	3. REPORT TYPE AND DATES COVERED
	15 July 1994	Progress Report: 01/16/94-07/15/94

4. TITLE AND SUBTITLE
Investigation of a Normal Incident High Performance P-type Strained Layer $In_{0.3}Ga_{0.7}As/In_{0.52}Ga_{0.48}As$ Quantum Well Infrared Photodetector

5. FUNDING NUMBERS
ONR #N00014-93-1-0827

6. AUTHOR(S)
Jerome T. Chu, Student
Sheng S. Li, Professor

7. PERFORMING ORGANIZATION NAME(S) AND ADDRESS(ES)
University of Florida
Gainesville, FL 32611-6200

8. PERFORMING ORGANIZATION REPORT NUMBER
92120712

9. SPONSORING/MONITORING AGENCY NAME(S) AND ADDRESS(ES)
US Navy, Office of Naval Research
800 North Quincy Street, Code 1512B:SM
Arlington, VA 22217-5000

10. SPONSORING/MONITORING AGENCY REPORT NUMBER

11. SUPPLEMENTARY NOTES

12a. DISTRIBUTION/AVAILABILITY STATEMENT
Approved for public release, distribution unlimited.

12b. DISTRIBUTION CODE

13. ABSTRACT *(Maximum 200 words)*

During this reporting period, we have made excellent progress towards the program goals. A significant achievement was made in the development of a new compressionally strained p-type GaAs/InGaAs QWIP grown on GaAs by MBE. This new QWIP achieved two color detection with detective peaks at 8.9 μm and 8.4 μm in the LWIR band and 5.5 μm in the MWIR band. This detector is under background limited performance (BLIP) at temperatures up to 70 K. The measured responsivity were found to be 24 mA/W and 45 mA/W for the two LWIR peaks respectively, while a responsivity of 13 mA/W was found for the MWIR peak; all at T=75 K. Additional characteriztion on the tensile strain InGaAs/InAlAs on InP P-QWIP has been performed and the results are summarized in this report. Currently, we are investigating other possible p-type QWIP structures with different performace parameters. These include a new dual strained InGaAs/InAlAs p-type QWIP. Additional consideration is being given towards the reliability of p-type contacts and the strained layer material for these QWIP structures.

14. SUBJECT TERMS	15. NUMBER OF PAGES
P-type strained layer InGaAs/InAlAs quantum well infrared photodetectors (QWIPs), intersubband absorption, dark current, responsivity, detectivity.	16. PRICE CODE

17. SECURITY CLASSIFICATION OF REPORT	18. SECURITY CLASSIFICATION OF THIS PAGE	19. SECURITY CLASSIFICATION OF ABSTRACT	20. LIMITATION OF ABSTRACT
Unclassified			Unlimited

Second Semi-Annual Progress Report (1/16/94-7/15/94)

Project Title: The Development of a Normal Incidence High Performance p-Type Strained Layer $In_{0.3}Ga_{0.7}As/In_{0.52}Al_{0.48}As$ Quantum Well Infrared Photodetectors

Program Manager: Max N. Yoder, Office of Naval Research, Code 3140, Arlington, VA.

Principal Investigator: Sheng S. Li, Professor, University of Florida, Gainesville, FL.

Student : Jerome T. Chu

Project Objective:

The objective of this project is to perform theoretical and experimental studies of dark current, photocurrent, optical absorption, spectral responsivity, noise, and detectivity for the normal incidence strained layer p-type III-V compound semiconductor quantum well infrared photodetectors (QWIPs) developed under this program. The material systems under investigation include InGaAs/InAlAs on InP substrates and GaAs/InGaAs on GaAs substrates. The project will study the usage and effects of biaxial tension and compressional strain on the material systems and their effects towards photodetector design.

I. Introduction

During the period of January 16, 1994 to July 15, 1994, significant progress has been made towards the design, fabrication, and characterization of strained layer p-type InGaAs/InAlAs on InP and GaAs/InGaAs on GaAs quantum-well infrared photodetectors (P-QWIPs) in the 8-14 μm range for staring focal plane arrays (FPAs). Specific tasks performed during this period include: (i) the continuing characterization and analysis of a normal incidence strained-layer p-type InGaAs/InAlAs QWIP on an InP substrate by molecular beam epitaxy (MBE) with peak detective wavelength at 8.1 μm, (ii) the design, growth, fabrication, and characterization of a normal incidence strained-layer p-type GaAs/InGaAs QWIP on a GaAs substrate with a peak long-wavelength infrared (LWIR) detective wavelength at 8.9 μm and a mid-wavelength infrared (MWIR) detective peak at 5.5 μm, (iii) the design, growth, fabrication, and preliminary characterization of a dual strained (both compressional and tensile strain are present) normal incidence p-type InGaAs/InAlAs QWIP with a LWIR peak at 10.2 μm. The following sections of this report will cover the technical results of the study so far and the research accomplishments and publications.

II. Technical Results

2.1 Research Accomplishments and Publications

1. Further characterization of the normal incident ultra-low dark current tensile strained InGaAs/InAlAs P-QWIP with a $\lambda_p = 8.1$ μm. The background limited detectivity was found to be 5.9x10^{10} cm-Hz$^{-1/2}$/W at 77 K with BLIP limited operation up to 90 K. These are the highest reported BLIP conditions for a QWIP. The results are summarized later in the text.

2. The design, growth, fabrication, and characterization of a compressively strained p-type InGaAs/GaAs QWIP on a GaAs substrate with peak wavelengths of $\lambda_{p1} = 8.9$ μm and $\lambda_{p2} = 5.5$ μm. Maximum responsivities of 93 mA/W and 30 mA/W were measured for each respective peak wavelength at 75 K. BLIP performance was achieved in the 8-14 μm long wavelength infrared (LWIR) detection band at 70 K and under 0.3 V of

applied bias.

3. The design, growth, fabrication, and characterization of a dual strain InGaAs/InAlAs P-QWIP with a peak wavelength of 10.2 μm. Preliminary data for this device will be discussed later in the text.

A. Journal Papers:

1. Y. H. Wang, S. S. Li, and J. Chu and Pin Ho, "An Ultra-low Dark Current P-type Strained-layer InGaAs/InAlAs Quantum Well Infrared Photodetector with Background Limited Performance (BLIP)" *Appl. Phys. Letts*, Feb. 7 issue, 1994.

2. Y. H. Wang, S. S. Li, and J. Chu and Pin Ho, "A Normal Incidence P-type Compressive Strained-Layer InGaAs/GaAs Quantum Well Infrared Photodetector for Mid-Wavelength Infrared (MWIR) and Long-Wacelength Infrared (LWIR) Detection" *J. Appl. Phys.*, accepted, July 1994.

B. Conference Presentations:

1. S. S. Li, J. Chu, and Y. H. Wang, "A Normal Incidence P-type Strained Layer InGaAs/InAlAs Quantum Well Infrared Photodetector with Background Limited Performance at 77 K", presented at the 1994 SPIE symposium, Orlando, FL, April 4-8, 1994.

2. Pin Ho, Y. H. Wang, S. S. Li, and J. Chu, "MBE Growth of P-type Strained-layer InGaAs/InAlAs QWIPs", MBE Conference, accepted, October 1994.

3. Y. H. Wang, J. Chu, S. S. Li, and Pin Ho, "A Normal Incidence P-type Compressive Strained-Layer InGaAs/GaAs Quantum Well Infrared Photodetector", 2nd. International Conference on 2-20 μm Wavelength Infrared Detectors and Arrays, Miami Beach, October 9-14, 1994.

4. S. S. Li, Y. H. Wang, and J. Chu, "A New Class of Normal Incidence Strained-Layer III-V Quantum Well Infrared Photodetectors", LEOS '94, Boston, October 31-November 3, 1994.

2.2 P-QWIP Operation and Design Theory

With the advent of advanced molecular beam expitaxial technologies, device structures utilizing heterostructure quantum wells have been heavily explored. N-type quantum well infrared photodetectors (QWIPs) have been extensively studied in the recent years[1-2,28]. These systems use GaAs/AlGaAs and InGaAs/InAlAs structures for detection in the 3 - 5 μm mid-wavelength infrared (MWIR) and 8 - 14 μm LWIR atmospheric transmission windows. Since n-type GaAs/InGaAs and InGaAs/InAlAs QWIPs have inherently low electron effective masses and high electron mobilities, they offer excellent infrared (IR) detection properties. Due to the quantum mechanical selection rules which prohibit normal incidence intersubband absorption, focal plane arrays (FPA) using n-type QWIPs must use either metal or dielectric gratings to couple normal incidence IR radiation into the quantum well[2-4]. In contrast, because of the mixing between the light hole and heavy hole states, normal incidence illumination is allowed for the intersubband transition in p-type QWIPs; thus eliminating the need for metal or dielectric grating couplers.

P-type QWIPs using valence intersubband transitions have been demonstrated[5-7] in lattice-matched GaAs/AlGaAs and InGaAs/InAlAs material systems. In general, intersubband transitions excited by normal incidence radiation in p-type quantum wells are allowed since a linear combination of p-like valence band Bloch states exists, which provides a nonzero coupling between the normal radiation field and valence band Bloch states. The strong mixing between the heavy hole and the light hole states greatly enhances intersubband absorption. The drawback of using lattice-matched systems is the fact that the intersubband transition occurs between the heavy hole ground states and the upper excited states. Because of the relatively large heavy hole effective mass when compared to the electron effective mass, relatively weak absorption and therefore similarly low responsivity is predicted in the IR wavelength range when compared to n-type QWIPs. In order to increase the absorption characterisitics and responsivity of P-QWIPs, biaxial stress is introduced into the well layers of the QWIP structure. If the intentionally introduced biaxial stress between the well layers and the barrier layers contained in the layer thickness (the total thickness of the wells and

barriers) in the P-QWIP structure is less than the critical thickness, then pseudomorphic or coherent heterointerfaces can be grown without the introduction of defects between the layers. Based upon the force balance model[8,29-30], the equilibrium critical layer thickness, L_c, for an epilayer with the lattice constant, a, grown on a substrate with a lattice constant, a_s, is given as

$$L_c = \left(\frac{a}{\sqrt{2}\delta_o}\right) \frac{1 - \nu \cos^2 \Theta}{8\pi(1+\nu)\cos\alpha} \left[1 + \ln(h\sqrt{2}/a)\right], \quad (1)$$

where h is the epilayer thickness, Θ is the angle between the dislocation line and the Burges' vector, α is the angle between the slip direction and the layer plane direction, δ_o is the lattice-mismatch or the in-plane strain, and ν is the Poisson ratio. δ_o is defined as $\delta_o = (a_s - a)/a$ where $\delta_o > 0$ for tensile strain and $\delta_o < 0$ for compressive strain. Similarly, ν is defined as $\nu = -C_{12}/C_{11}$. C_{ij}'s are the elastic constants and can be found in reference 9.

The strained-layers have the same effective in-plane lattice constant, $a_{||}$ (i.e., $a_{x,y}$), and can store the excess energy due to the elastic strain within the layers. The in-plane lattice constant, $a_{||}$, can be expressed by[8]

$$a_{||} = a_1 \left[1 + \delta_o / \left(1 + \frac{\xi_1 L_1}{\xi_2 L_2}\right)\right], \quad (2)$$

where $a_{1,2}$ and $L_{1,2}$ are the individual layer lattice constants and thicknesses, respectively, and $\xi_{1,2}$ are the shear moduli as described by $\xi = (C_{11} + C_{12} - 2C_{12}^2/C_{11})$, where the C_{ij}'s are elastic constants for the strained material. δ_o denotes the lattice mismatch between layers and $a_{1,2}$ are the lattice constants of the strained well and the substrate (or barrier) respectively. When $a_{||} \neq a_s$, the coherently strained superlattice structure is no longer in equilibrium with the substrate. If the lattice constant of the barrier layers is equal to that of the substrate, the the strain wili be completely accomodated in the well layers with no strain in the barrier layers. However, Hull et al.[22] showed that if the individual layers thicknesses in the superlattice is less than its critical thickness, even though $a_{||} \neq a_s$, the loss of coherence only occurs at the interface between the whole superlattice and the substrate, while the superlattice itself remains coherent.

If the QWIP structure is grown along the [100] direction and the strained-layer is within the critical thickness, L_c, then a pseudomorphic or coherent heterointerface can be obtained and the components of the strain tensor [e] are simplified to the expressions given by

$$e_{xx} = e_{yy} = e_{||} \quad (3)$$

$$e_{zz} = -e_{\|}\left(\frac{2C_{12}}{C_{11}}\right) \quad (4)$$

$$e_{xy} = e_{yz} = e_{zx} = 0. \quad (5)$$

In addition to altering the physical parameters of the QWIP, lattice strain can also induce energy band shifts, which can be used to alter the absorption characteristics of the QWIP. The strain induced energy band shifts for the conduction band, the heavy hole subband, and light hole subband can be approximated as follows.

$$\Delta E_c = 2c_1\frac{C_{11}-C_{12}}{C_{11}}\delta_o \quad (6)$$

$$\Delta E_{hh} = b\frac{C_{11}+C_{12}}{C_{11}}\delta_o \quad (7)$$

$$\Delta E_{lh} = -\Delta E_{hh} + \frac{(\Delta E_{hh})^2}{2\Delta_o} \quad (8)$$

where c_1 is the combined hydrostatic deformation potential which characterizes the splitting of the Γ_8 valence band under strain and b is the shear deformation potential and Δ_o is the spin orbit split-off energy[9]. The total hydrostatic deformation potential ($c_1 + V_v$), where V_v is the valence band deformation potential, can be expressed by[10]

$$c_1 + V_v = -\frac{1}{3}(C_{11} + 2C_{12})\frac{dE_g^o}{dP}, \quad (9)$$

where dE_g^o/dP is the unstrained energy bandgap change with respect to the unit pressure.

The effect of strain on the energy band structure results in the splitting of the heavy hole and light hole band at the valence band zone center[11] (i.e., the in-plane wavevector $k_{\|} = 0$), which is degenerate in the unstrained case. When tensile strain is applied between the quantum well and the barrier layers[12-14] along the superlattice growth z-direction, the strain can push the light hole levels upwards and pull the heavy hole levels downwards. We can therefore expect that heavy hole and light hole states can be inverted at specific lattice strains and quantum well thicknesses. This phenomena will in turn cause the intersubband transitions in a QWIP structure to take place from the populated light hole ground state to the upper energy band states. Since the light hole has a small effective mass (comparable to the electron effective mass), the optical absorption and photon responsivity in p-type QWIPs can be greatly enhanced, as a result of introducing strain in the quantum well. In addition to the utilization of the light hole states for their small effective masses, etc., certain

heavy hole states under compressional strain may also have similar characteristics, like high mobilities, small effective masses, and long mean free paths; which in turn favorably alter the intersubband absorbtion and transport characteristics, as shown by Hirose, et al.[31].

To calculate the locations of the energy subbands, we can use the transfer matrix method (TMM)[13,15], based on the eight-band $\mathbf{k} \cdot \mathbf{p}$ model. This model is represented by the Luttinger-Kohn Hamiltonian[16-17], H_t, which describes the unstrained semiconductor.

$$H_t = H + V(z) \tag{10}$$

where

$$H = \begin{bmatrix} H_{11} & H_{12} & H_{13} & H_{14} \\ H_{21} & H_{22} & H_{23} & H_{24} \\ H_{31} & H_{32} & H_{33} & H_{34} \\ H_{41} & H_{42} & H_{43} & H_{44} \end{bmatrix} \tag{11}$$

with:

$$H_{11} = \tfrac{\gamma_1+\gamma_2}{2}(k_x^2 + k_y^2) + \tfrac{\gamma_1-\gamma_2}{2}k_z^2$$

$$H_{22} = \tfrac{\gamma_1-\gamma_2}{2}(k_x^2 + K_y^2) + \tfrac{\gamma_1+\gamma_2}{2}k_z^2$$

$$H_{12} = i\sqrt{3}\gamma_3(k_x - ik_y)k_z$$

$$H_{13} = \tfrac{\gamma_2\sqrt{3}}{2}(k_x^2 - k_y^2) - i\sqrt{3}\gamma_3 k_x k_y$$

$$H_{21} = H_{12'}^* \qquad H_{13} = H_{31'}^* \qquad H_{24} = H_{13}$$

$$H_{34} = H_{12'} \qquad H_{42}^* = H_{13'}^* \qquad H_{43} = H_{12}^*$$

$$H_{14} = H_{23} = H_{32} = H_{41} = 0$$

and V(z) is a step function where V(z) vanishes inside the well layers and equals V_o in the barrier layers. The effect of strain is included by adding the Pikus-Bir Hamiltonian[18], H_s, to the general Luttinger-Kohn Hamiltonian. As shown below, the strain Hamiltonian for the well material is a diagonal matrix.

$$H_s = \begin{bmatrix} -\Delta E_c - \Delta E_{hh} & 0 & 0 & 0 \\ 0 & -\Delta E_c + \Delta E_{hh} & 0 & 0 \\ 0 & 0 & -\Delta E_c + \Delta E_{hh} & 0 \\ 0 & 0 & 0 & \Delta E_c + \Delta E_{hh} \end{bmatrix} \tag{12}$$

Using the aforementioned techniques, we can numerically calculate the energy of the zone-center valence subband levels as a function of well width for any material system under tensile or compressional strain and also determine the change in the valence subband structures.

All of the previously described calculations are derived from the multiband effective mass $\mathbf{k}\cdot\mathbf{p}$ model for a coherently strained structure, which is based upon the perturbation approximation. In the $\mathbf{k}\cdot\mathbf{p}$ model, the interactions of S-P type coupling among conduction (C), light-hole (LH), heavy-hole (HH), and spin-orbit (SO) states combined with spin-orbit like coupling are taking into consideration to derive the band structures. This results in an 8×8 $\mathbf{k}\cdot\mathbf{p}$ Hamiltonian and momentum matrix elements. Using the pertubation approximation, a set of wave functions of $S_{1/2}$: $|1/2,\pm1/2>_c$; $P_{3/2}$: $|3/2,\pm3/2>$, $|3/2,\pm1/2>$; and $P_{1/2}$: $|1/2,\pm1/2>$ are used to represent the unperturbed and unstrained basis in the $|J,m_j>$ presention[23]. $m_j=\pm1/2$ represents either the electron or LH states, while $m_j=\pm3/2$ denotes the HH or heavy particle states. A slightly simplified 6×6 $\mathbf{k}\cdot\mathbf{p}$ Hamiltonian can be used to roughly predict the P-like properties of the coherently strained layers by considering the S-like conduction band states as a pertubation, if a large enough bandgap exists, like in InGaAs and GaAs layers. The wave functions of the coherently strained superlattice at the zone center ($\mathbf{k}=0$) are given by[24]

$$|3/2,\pm3/2> \quad HH states \tag{13}$$

$$\gamma|3/2,\pm1/2>+\ \beta|1/2,\pm1/2> \quad LH states \tag{14}$$

$$-\beta|3/2,\pm1/2>+\ \gamma|1/2,\pm1/2> \quad SO states \tag{15}$$

where γ and β are constants which are dependent on the strain parameters. Note that the heavy-hole states, $|3/2,\pm3/2>$, are still decoupled from the other valence band states even under biaxial stress at the zone center, while the light-hole and spin-orbit split off states are coupled at $\mathbf{k}=0$. However, the HH, LH, and SO states are mixed[25,26] in the coherently strained superlattice at off zone center ($\mathbf{k}\neq0$). This mixing between the states with different m_j's is due to the boundary conditions across the interface of the quantum well layers. By examining the $\mathbf{k}\cdot\mathbf{p}$ matrix, we can see that the interaction between the different m_j states is proportional to the transverse components of the wave vector, $k_{x,y}$, so that the HH states are decoupled when $k_{x,y}=0$. It is interesting to note that the $k_{x,y}$'s are conserved across the interfaces since the interface potential depends only on z, the quantum well growth

direction. Thus the band mixing can be significant if the Γ-bandgap is small, like with GaAs and InGaAs, and if the LH and SO bands involved in the transition have a large k_z value[25].

Since the heavy hole and light hole valence subbands are non-degenerate following the introduction of strain into the QWIP structure, a simpler method can be used to determine the energies of the subbands. By using the parabolic band approximation near the valence band zone-center, and the energy band shifts for the conduction band minimum, heavy hole subband maximum, and light hole subband maximum, we can utilize the simpler two-band Hamiltonian for electrons just by finding the effective mass of the carriers (i.e., heavy hole effective mass and light hole effective mass) and the barrier heights for each carrier type. Although this does not simultaneously determine the energy levels of both carriers, it does allow accurate predictions of the energy subbands. When compared to the direct calculation of the energy subbands, the two-band approximation yields accurate results when compared to the direct calculation results[13,18] (see also figures 1(a)-1(c)). One limitation of the TMM is that this method cannot calculate the energy levels of the allowed energy subbands in the continuum states. In order to determine the transition energy from the ground state to the continuous state, we used the Kronig-Penney model to determine the locations of the allowed energy bands in the continuum states.

As can be seen in figures 1(b) and 1(c), the influence of strain on the relative positions of the heavy hole (HH) and light hole (LH) subbands is apparent. When a biaxial internal tension is applied to the well material (in this case $Ga_{0.7}In_{0.3}As$ on an InP substrate with the barrier layers consisting of lattice matched $Al_{0.48}In_{0.52}As$), the strain pulls the LH subbands up with respect to the HH subbands for a given well thickness. While quantum confinement effects tend to push the LH subbands down with respect to the HH subbands. As the well width is increased above a certain value, the strain effect can overcome the quantum confinement effect and therefore induce the inversion of the heavy hole and light hole subbands at the ground state. In contrast, with the application of compressional strain on the well layers, as we see in the $In_{0.4}Ga_{0.6}As/GaAs$ quantum well structure, the strain pushes the LH subbands down with respect to the HH subbands for a given well thickness.

In addition to the energy level and energy band locations, the calculation of intersubband and interband transitions are also of great interest. In order to determine the intersubband and interband transitions in a p-type strained layer QWIP, the usage of the

6×6 Hamiltonian which includes the previously mentioned $\mathbf{k}\cdot\mathbf{p}$ Hamiltonian[16-17,24] and the strain Hamiltonian[18]. Since the strain and the pin-orbit coupling terms do not life the spin degeneracy, the 6×6 Hamiltonian matrix can then be factorized into two 3×3 irreducible matrices. The assumption that the Fermi distribution function if equal to one for the confined ground state and is equal to zero for the excited states in equilibrium is used to simplify the calculation without loss of accuracy. The absorption coefficient for the intersubband or interband transition between the initial ground state, i, and the final continuum state, f, is given by[27]

$$\alpha_i(\omega) = \sum_f \frac{4\pi^2 e^2}{n_r c m_o^2 \omega} \int_{BZ} \frac{2d\mathbf{k}}{(2\pi)^3} \left[(f_i - f_f) |\hat{\epsilon}\cdot\mathbf{P}_{i,f}|^2 \frac{\Gamma/2\pi}{[\Delta_{i,f}(\mathbf{k}) - \hbar\omega]^2 + (\Gamma^2/4)} \right] \tag{16}$$

where n_r is the refractive index in the quantum well, m_o is the free electron mass, $\Delta_{i,f}$ is the energy difference between the initial ground state, i, of energy $E_i(\mathbf{k})$ and the final state, f, with the corresponding energy of $E_f(\mathbf{k})$. $\hat{\epsilon}$ and ω are the unit polarization vector and the frequency of the incident IR radiation, respectively, f_i and f_f are the Fermi distribution functions of the initial and final states, and Γ is the full width of level broadening. $\Gamma \sim \hbar/\tau_{if}$, where τ_{if} is the lifetime between the initial, i, and final, f, states. $|\hat{\epsilon}\cdot\mathbf{P}_{i,f}|$ are the optical transition elements between the quantum well valence subband ground states, i, and the continuum subband states, f, in the HH, LH, and SO bands; which can be derived from the two 3×3 $\mathbf{k}\cdot\mathbf{p}$ matrix elements as shown below.

Using the following 3×3 optical matrix,

$$\frac{m_o}{\hbar} \begin{bmatrix} T_{HH} & T_{HL} & T_{HS} \\ T_{LH} & T_{LL} & T_{LS} \\ T_{SH} & T_{SL} & T_{SS} \end{bmatrix}, \tag{17}$$

the optical matrix elements, $|\hat{\epsilon}\cdot\mathbf{P}_{i,f}|$, can be obtained. These matrix elements have the same form as the $\mathbf{k}\cdot\mathbf{p}$ matrix elements except that the $k_i k_j$'s are replaced with $k_i\epsilon_j + k_j\epsilon_i$ multiplied by a constant factor of $m_o/\hbar$.[27] The T_{ij}'s are defined as follows:

$$T_{HH} = 2(A-B)\epsilon_z k_z + (2A+B)(\epsilon_x k_x + \epsilon_y k_y), \tag{18}$$

$$T_{LL} = 2(A+B)\epsilon_z k_z + (2A-B)(\epsilon_x k_x + \epsilon_y k_y), \tag{19}$$

$$T_{SS} = 2A(\epsilon_x k_x + \epsilon_y k_y + \epsilon_z k_z) \tag{20}$$

$$T_{HL} = i\frac{1}{\sqrt{3}} N(\epsilon_x \cos\eta - \epsilon_y \sin\eta) k_z - i\frac{1}{3} N \epsilon_z k_{\|}$$

$$
\begin{aligned}
& -\sqrt{3}B(\epsilon_x k_x - \epsilon_y k_y)\cos\chi \\
& +\frac{1}{\sqrt{3}}N(\epsilon_x k_y + \epsilon_y k_x)\sin\chi, && (21)
\end{aligned}
$$

$$
\begin{aligned}
T_{HS} &= \frac{1}{\sqrt{6}}N(\epsilon_x\cos\eta + \epsilon_y\sin\eta)k_z + \frac{1}{6}N\epsilon_z k_{\|} \\
& +i\sqrt{6}B(\epsilon_x k_x - \epsilon_y k_y)\cos\chi \\
& -\frac{2}{\sqrt{6}}N(\epsilon_x k_y + \epsilon_y k_x)\sin\chi, && (22)
\end{aligned}
$$

$$
\begin{aligned}
T_{LS} &= \left[i2\sqrt{2}B\epsilon_z + \frac{1}{\sqrt{2}}N\epsilon_x\cos(\chi-\eta) - \epsilon_y\sin(\chi-\eta)\right]k_z \\
& -i\sqrt{2}B(\epsilon_x k_x + \epsilon_y k_y) \\
& -\frac{1}{\sqrt{2}}N\epsilon_z k_{\|}\cos(\chi - 2\eta), && (23)
\end{aligned}
$$

$$
T_{SH} = T^*_{HS}, \qquad (24)
$$

$$
T_{SL} = T^*_{LS}, \qquad (25)
$$

$$
T^*_{LH} = T^*_{HL}. \qquad (26)
$$

Here A, B, N, χ, η are inverse mass band parameters.[27]

Although our band structure and absorption calculations can be used to determine the positions of the subbands in the quantum wells, and hence determine the peak absorption wavelength of the QWIP, many other factors must be taken into account to create a successful detector. Generally, for a useful detector, the responsivity must be high, while the noise current must be low. The responsivity, R, for a photodetector may be expressed as[19]

$$
R = \frac{q\lambda\eta p}{hc}G, \qquad (27)
$$

where q is the electronic charge, λ is the wavelength of the incident photon, h is the Planck constant, c is the speed of light, p is the tunneling probability out of the quantum well, η is the quantum efficiency and the photoconductive gain is G. The quantum efficiency and photoconductive gain are described, respectively, by[19]

$$
\eta = A\left[1 - exp\left(-B\alpha l_{qw}\right)\right] \qquad (28)
$$

$$
G = \frac{L}{t_c} \qquad (29)
$$

where A is a constant that is polarization dependent, α is the absorption coefficient of the quantum well, l_{qw} is the total width of all quantum well regions, L is the mean free path

of the carrier, and t_c is the total width of all quantum well and barrier regions. B is a constant dependent on the number of passes IR radiation makes through the photodetector. For n-type QWIPs, A=0.5, while for p-type QWIPs A=1. The mean free path of the carrier may be expressed as[19]

$$L = \tau T_{qw} \mu_{eff} E, \tag{30}$$

where τ is the well recapture lifetime of the carrier, T_{qw} is the transmission coefficient over the quantum well, μ_{eff} is the effective mobility of the carrier, and E is the electric field. The effective mobility for a two-band transport model is shown to be[19]

$$\mu_{eff} = \frac{\Delta p_{lh} \mu_{lh} + \Delta p_{hh} \mu_{hh}}{\Delta p_{lh} + \Delta p_{hh}}, \tag{31}$$

where Δp_{hh} and Δp_{lh} are the concentrations of optically induced heavy and light hole carriers respectively, and μ_{hh} and μ_{lh} are the respective heavy and light hole mobilities. When only the ground state is completely occupied, either Δp_{lh} or Δp_{hh}, the optically induced light holes or the optically induced heavy holes dominate, so that we may estimate μ_{eff} as the in-plane effective mass of the ground state carriers.

Another important parameter to be considered in a QWIP design is the dark current density (J_d), which is expressed using the Richardson-Dushman equation[14] as

$$J_d \propto T^2 m^* exp\left(\frac{-\Delta E}{kT}\right), \tag{32}$$

where m^* is the effective mass, ΔE is the difference in energy between the barrier height and the quantum confined state in the well, k is the Boltzmann constant, and T is the temperature.

The noise in QWIP structures is mainly due to random fluctuations of thermally excited carriers. The noise is expressed as[5]

$$i_{noise} = \sqrt{4 A_d q G \Delta f J_d}, \tag{33}$$

where A_d is the detector area, and Δf id the bandwidth. Finally, a figure of merit measurement used to compare detectors is the detectivity, D^*, which is shown to be[19]

$$D^* = \sqrt{A_d \Delta f} \frac{R}{i_{noise}}. \tag{34}$$

If the dark current in a particular QWIP is lower than the 300 K background photocurrent, then the QWIP can be considered to be under background limited performance (BLIP). In a BLIP limited QWIP, the dominant current is due to photon noise, since all the other sources are negligible by comparison. The photon noise is calculated from the arrival statistics of the incoherent photons. The background photon noise current, i_{np}, is given by[20,21]

$$i_{np}^2 = 4Aq^2\eta g^2 P_b B/(h\nu), \tag{35}$$

where P_b is the incident background optical power, B is the QWIP bandwidth, η is the absorption quantum efficiency, ν is the incident photon frequency, and g is the photoconductive gain. The photocurrent, I_p can be approximated by

$$I_p = A(q/h\nu)\eta g P_s, \tag{36}$$

where P_s is the incident optical signal power. The constant, A, in Eqs. (35) and (36), is due to the polarization selectivity for n-type QWIPs versus p-type QWIPs. As previously stated, for n-type QWIPs, A = 0.5, while A = 1 for p-type QWIPs. By setting the signal-to-noise power ratio equal to unity, the background limited noise equivalent power, $(NEP)_{BLIP}$ and the detectivity, D^*_{BLIP}, can be expressed as follows for n-type QWIPs.

$$(NEP)_{BLIP} = 2\sqrt{2h\nu B P_b/\eta} \tag{37}$$

$$D^*_{BLIP} = \sqrt{A_d B}/(NEP)_{BLIP} = \frac{\lambda_p}{2\sqrt{2}hc}\left(\frac{\eta}{Q_b}\right)^{1/2}, \tag{38}$$

where A_d is the active area of the detector, and $Q_b = P_b/(Ah\nu)$ is the incident photon flux from the background for a given spectral bandwidth, $\Delta\nu$, and a peak wavelength, λ_p. Q_b is defined as

$$Q_b = \frac{2\pi}{c^2}\frac{\nu^2\Delta\nu}{e^{h\nu/k_bT}-1} sin^2\left(\frac{\theta}{2}\right), \tag{39}$$

where, θ, is the field of view (FOV). For a p-type QWIP, a factor of $\sqrt{2}$ is used in the denominator of Eq. (38), D^*_{BLIP}, since it can absorb both optical polarizations of the incident IR radiation.

2.3 Characterization of Strained Layer P-QWIPs

2.3.1 An $In_{0.3}Ga_{0.7}As/In_{0.52}Al_{0.48}As$ on InP P-QWIP with Tensile Strain

As can be seen in figures 1(b) and 1(c), we can utilize the strain inherent in a lattice mismatched system in addition to the engineering of the well thicknesses and barrier layers to modify the energy band structure of the p-type QWIPs. The strained-layer $In_{0.3}Ga_{0.7}As/In_{0.52}Al_{0.48}As$ P-QWIP as shown in figure 1(a), uses a light hole ground state to heavy hole continuum state intersubband transition for IR detection. The QWIP structure was grown on a (100) semi-insulating (SI) InP substrate via molecular beam expitaxy (MBE). Beryllium was used as the p-type dopant and the structure consists of 20 periods of 40 $\AA$ thick $In_{0.3}Ga_{0.7}As$ quantum wells with a dopant density of $1x10^{18}$ cm^{-3} seperated by 450 $\AA$ thick barrier layers of undoped $In_{0.52}Al_{0.48}As$ barrier layers. A 0.3 μm thick cap layer and a 1 μm thick buffer layer of lattice-matched $In_{0.53}Ga_{0.47}As$ were grown with a dopant density of $2x10^{18}$ cm^{-3} to serve as ohmic contacts. The contact and barrier layers were designed to be lattice matched with the InP substrate. The quantum wells are in biaxial tension with a lattice mismatch of 1.6% between the well layers and the substrate. A 200 μm by 200 μm mesa was then created by chemical etching to facilitate the measurement of spectral responsivity and dark current of the QWIP. Since the dopant density in the ohmic contact cap and buffer regions were slightly less than that required for using Au/Cr contacts, an Au/Zn alloy was used to make ohmic contacts to the p-type QWIP. The ohmic contacts were thermally evaporated onto the QWIP mesas to a thickness of approximately 1200 $\AA$. The QWIPs were annealed at 480 °C for two minutes to obtain stable and low contact resistances.

Figure 2(b) shows the measured dark current density from 77 K to 110 K with a 300 K background photocurrent superimposed. The asymmetric dark current characteristic in this p-type QWIP was observed due to the band bending in the barrier layers as shown in Fig. 1(a). Due to the extremely low dark current density of this QWIP, it is under background limited performance (BLIP) for a field of view (FOV) of 90° at a temperature less than 90 K under applied biases from -2.5 V to +5 V and higher. In the forward biased regime, the QWIP is under BLIP operation up to 100 K with an applied bias of +2.5 V. Figure 2(a) shows the calculated absorption coefficient at normal incidence for a SL P-QWIP with a 6 nm well thickness versus that of an unstrained P-QWIP.

The responsivity of the QWIP can be measured as a function of temperature, applied bias, and incident radiation wavelength. Using a globar and an automatic PC-controlled sin-

gle grating monochrometer, under normal incidence infrared (IR) radiation, we can measure the photocurrent versus radiation wavelength for both positive and negative biases; which are shown in figures 3(a) and 3(b), respectively. A peak wavelength at λ_p=8.1 μm was observed in the LWIR detection band, which is attributed to the intersubband transition between the confined ground light hole state, E_{LH1}, and the continuum heavy hole states, E_{HH3}. The cutoff wavelength was found to be 8.8 μm which corresponds to a spectral bandwidth of $\Delta\lambda/\lambda_p$ = 12%. The responsivities for the p-type QWIP were calibrated using a standard pyroelectric detector and lock-in amplifier. Asymmetric responsivities of 34 mA/W and 51 mA/W at +4 V and -4 V bias, respectively, were measured. The maximum BLIP detec D^*_{BLIP}, at λ_p=8.1 μm was determined to be 5.9x10^{10} cm-Hz$^{1/2}$/W with a responsivity, R_i 18 mA/W at +2 V bias with a FOV = 90° at 77 K. The quantum efficiency for the p-type QWIP was estimated from the responsivity measurements using a conservative photoconductive gain estimate of g=0.015. The %BLIP can be evaluated as follows when the Johnson noise and readout noise are ignored; with i_{np} and i_{nd} are the 300 K background photocurrent noise and dark current noise, respectively.

$$\%BLIP \approx \frac{i_{np}}{(i_{np}^2 + i_{nd}^2)^{1/2}} \tag{40}$$

Using the above expression, a nearly full BLIP detection was achieved at biases with magnitudes less than 2 V, as seen in figure 4. Due to the BLIP detection, the noise equivalent temperature difference (NEΔT) is expected to be improved significantly for this QWIP.

The temperature dependence of the responsivity and detectivity was also explored for this $In_{0.3}Ga_{0.7}As/In_{0.52}Al_{0.48}As$ SL P-QWIP. Due to the non-uniformities across the QWIP wafer, the peak responsivities and detectivities varied from device to device. As illustrated by figure 5, the responsivity increases with increased applied bias at each temperature. For applied biases above 3 V at 100 K, the sudden drop in responsivity can be attributed to the onset of non-BLIP operation, as also indicated in figure 2(b). The calculated detectivity at 2 V and 4 V of applied bias for this device at temperatures ranging from 77 K to 100 K is presented in table 1. As expected, the detectivity decreases as the temperature increases above 77 K, since the inherent dark current density is rapidly increasing with the increasing ambient temperature and larger applied bias.

2.3.2 An $In_{0.4}Ga_{0.6}As/GaAs$ on GaAs P-QWIP with compressional strain

Unlike the $In_{0.3}Ga_{0.7}As/In_{0.52}Al_{0.48}As$ on InP P-QWIP with tensile strain between the layers, a normal incidence $In_{0.4}Ga_{0.6}As/GaAs$ on GaAs P-QWIP was designed for two color detection in the 3-5 μm MWIR and 8-14 μm LWIR bands. With this device, we have demonstrated two color detection in p-type strained-layer QWIPs for the first time.

The p-type compressively strained $In_{0.4}Ga_{0.6}As/GaAs$ QWIP was grown on a semi-insulating (SI) GaAs substrate via molecular beam epitaxy (MBE). This QWIP structure consists of 20 periods of 40 $\AA$ $In_{0.4}Ga_{0.6}As$ quantum well Be-doped to a density of 4×10^{18} cm^{-3} separated by a 350 $\AA$ wide barrier layer of undoped GaAs. A 0.3 μm cap layer and a 1.0 μm buffer layer of Be-doped GaAs with a dopant density of 5×10^{18} cm^{-3} were grown to serve as top and bottom ohmic contacts. The contact and barrier layers are lattice matched with the SI GaAs substrate, while the $In_{0.4}Ga_{0.6}As$ quantum well layers are under biaxial compression with a designed lattice mismatch of approximately 2.8%. Due to the heavily doped large-bandgap contact layers of this P-QWIP, a large tunneling current from the triangle potential near the ohmic contact region may be dominant with respect to the QWIP's dark current. Therefore a relatively thick (550 $\AA$) undoped GaAs barrier layer was grown next to the top and bottom contact layers to reduce this dark current component.

To facilitate the characterization of this P-QWIP, a 200×200 μm^2 mesa structure was created by wet chemical etching. An Au/Cr film was deposited onto the QWIP mesas and the buffer layer via e-beam deposition with a thickness of approximately 1500 $\AA$ for ohmic contacts. The semi-insulating GaAs substrate was thinned down to approximately 50 μm to lower the substrate absorption screening effect, and polished to a mirror-like surface to reduce the reflection of the normal incidence IR radiation.

Figures 6(a) and 6(b) show the idealized energy band diagram and energy subband states for the compressively strained P-QWIP. In this case, the intersubband transitions are from the highly populated heavy hole ground state (E_{HH1}) to the upper heavy hole continuum states (E_{HH3} and E_{HH4}) for the 8.9 μm LWIR detection peak and the 5.5 μm MWIR detection peak, respectively.

The mobility of the heavy-hole is enhanced by the compressive strain in the $In_{0.4}Ga_{0.6}As$ quantum well due to the reduction of heavy hole effective mass by a factor of three[31]. Another effect attributed to the compressional strain localized in the quantum well is the decrease of the density of states in the well. This causes more heavy holes to reside in higher energy

states, which effectively raises the Fermi level when compared with the same unstrained quantum well. The raised Fermi level will cause an increase in the number of off-center (i.e., $\mathbf{k} \neq 0$) free heavy holes with lighter effective mass; which in turn causes a larger intersubband absorption when exposed to normal incidence IR radiation. Our InGaAs/GaAs compressional strain P-QWIP has its heavy holes in type-I band alignment, while the light holes are in the type-II band configuration. The binary GaAs layer used as the barrier layer should also exhibit superior current transport characterisitics when compared to a ternary barrier. Finally, the heavy hole excited continuum states are resonantly lined up with the light hole states; which gives rise to a strong quantum coupling effect. This resonant lined up effect makes the conducting holes behave like light holes. These resonant heavy holes exhibit high mobilities, small effective masses, and long mean free paths. Therefore, larger photoconductive gain and higher photoconductivity are expected for a compressively strained P-QWIP when compared with an unstrained one.

When compared with the $In_{0.3}Ga_{0.7}As/In_{0.52}Al_{0.48}As$ tensile strain P-QWIP, the measured dark current at various temperatures is much higher (see figure 7). This device also exhibits an asymmetrical dark current characteristic, like the InGaAs/InAlAs tensile strain P-QWIP, which can be attributed to the dopant migration effect which occurs during layer growth[32]. For a field of view (FOV) of 90° the InGaAs/GaAs compressionally strained P-QWIP is under background limited performance (BLIP) at V_b = 0.3 V, T = 70 K and V_b = 0.7 V, T = 55 K.

The responsivity of this QWIP was measured under normal incidence illumination as a function of temperature, applied bias, and incident IR wavelength using a blackbody radiation source and automatic PC-controlled single grating monochrometer system. Twin LWIR peaks were detected at λ_{p1} = 8.9 μm and λ_{p2} = 8.4 μm as shown in figure 8(a). A single MWIR peak was discovered at λ_{p3} = 5.5 μm as seen in figure 8(b). At each peak wavelength, responsivities were measured as 24 mA/W at V_b = 0.3 V and 45 mA/W at V_b = 0.7 V for T $\leq$ 75 K. The twin LWIR peaks covered a broad wavelength band ranging from 6.5 to 12 μm. The cut-off wavelength for the LWIR band was found to be $\lambda_c \approx 10$ μm, which corresponds to a spectral bandwidth of $\Delta\lambda/\lambda_p$ = 35 %. The twin peak wavelengths are attributed to the intersubband transition from the confined ground heavy hole state (E_{HH1}) to the continuum heavy hole states (E_{HH3}), which is resonantly lined up with the type-II light

hole continuum states. The transition energies for the 8.9 μm and 8.4 μm peak wavelengths are in reasonable agreement with our theoretical calculations. While the physical origins of the twin LWIR peaks is not clear, a possible explanation can be given as follows. When the HH and LH bands in the continuum are strongly mixed, either individual subband can further split into two sub-subbands due to coupling or interaction, with one shifting up in energy and the other shifting down in energy. This gives rise to the observed twin detection peaks in the LWIR band. The MWIR peak observed at 5.5 μm had a wavelength bandwidth ranging from 4 to 6.5 μm. The measured responsivities of the MWIR band were found to be 7 mA/W and 13 mA/W at V_b = 0.3, 0.7 V and T = 75 K, respectively. The spectral bandwidth of $\Delta\lambda/\lambda_{p3}$ = 27 % was obtained with the cut-off wavelength at λ_c = 6 μm. The MWIR detection is attributed to the intersubband transition between the ground heavy hole state (E_{HH1}) and the upper continuum heavy hole state (E_{HH4}). In this case, no mixing or interaction between the HH and LH subbands was observed. A probable explanation is that the weak overlap interaction at higher subband levels prevents the sub-subband formation.

Responsivities for this compressively strained P-QWIP were measured at T = 75 K, and the results are shown in figure 9(a). The responsivity of the twin peak (either λ_{p1} = 8.9 μm or λ_{p2} = 8.4 μm) LWIR band increases almost linearly with bias voltage for $V_b \geq$ -1.6 V and $V_b \leq$ +1.2 V, which then rapidly falls to zero from the maximum responsivity within a voltage change of |0.1 V|. A similar photoresponse was obtained for the detective peak at λ_{p3} = 5.5 μm, as shown in figure 9(b). The gain has a maximum value of 0.13 at V_b = 1.6 V, and then rapidly falls to zero. This is due to the resonant transport coupling between the type-I heavy hole and type-II light hole states. The linear photoresponse exhibited by this device is due to the photoconductive gain which varies linearly with bias. So as the bias voltage increases, the resonant transport coupling breaks down, which causes the massive decrease in photoconductive gain leading to the lack of photocurrent when the applied bias is greater than 1.6 V. The maximum gain, g = 0.13, is the highest value ever reported in a P-QWIP.

2.3.3 An InGaAs/InAlAs on InP P-QWIP with dual strain layers

The $In_{0.3}Ga_{0.7}As/In_{0.65}Al_{0.35}As$ P-QWIP structure on InP was designed to explore the characteristics of a dually strained (tensile and compressive strain) detector. With this

device, we seek to demonstrate a low-dark current, high BLIP temperature P-QWIP with a detective peak at 10.2 μm in the LWIR band.

The p-type dually strained $In_{0.3}Ga_{0.7}As/In_{0.65}Al_{0.35}As$ QWIP was grown on a semi-insulating InP substrate by MBE technique. The QWIP consists of ten layers of 60 $\AA$ $In_{0.3}Ga_{0.7}As$ quantum wells Be-doped at a density of 2×10^{18} cm^{-3} seperated by a 360 $\AA$ thick undoped barrier composed of $In_{0.65}Al_{0.35}As$. A 0.3 μm thick layer of lattice matched $In_{0.53}Ga_{0.47}As$ Be-doped to a density of 4×10^{18} cm^{-3} was grown on top of the quantum wells to serve as the top ohmic contact. A similar 0.5 μm thick layer was grown under the quantum wells to serve as the bottom ohmic contact. The barrier layers are under biaxial compression with a designed lattice mismatch of 0.8% relative to the SI InP substrate, while the quantum well layers are under biaxial tension with a lattice mismatch of 1.65% when compared with the SI InP substrate.

Like the previous device structures, 200×200 μm^2 mesas were created by wet chemical etching. An Au/Zn film was deposited onto the P-QWIP mesa and buffer layer to a thickness of 1500 $\AA$ via thermal evaporation for use as an ohmic contact and as a reflective coating to improve the quantum efficiency of the P-QWIP. The Au/Zn contacts were then annealed at 450 °C for 60 seconds. The SI InP substrate was then thinned down to less than 50 μm to lower the substrate screening effect and create a waveguide-like layer between the ambient and the P-QWIP. The substrate was then polished to a mirror-like surface to reduce the reflection of the normal incidence IR radiation.

Our preliminary data indicates that the device is under BLIP conditions at 77 K under all applied biases from -1.0 to 1.0 volts (see figure 9). Since the dark current measured at 77 K is almost two orders of magnitude lower than the 300 K background photocurrent, the detector is expected to be under the BLIP condition at even higher device temperatures. Slightly asymmetrical and low dark currents at 77 K are also indicated. This slight asymmetry can be attributed to band bending of the layers due to the doping migration effect, as described in the previous sections. Complete measurements and analyses of the dark current, background photocurrent, photoresponse, and detectivity are currently underway.

2.4 Conclusion and Remarks

Over the last half-year period, we have achieved a greater understanding in regards to

the design and characterization of P-QWIPs. We have demonstrated a novel strained-layer design that utilizes biaxial tension on an InP substrate with ultra-low dark current, high detectivity, high responsivity, and BLIP operation. We have also demonstrated a reliable, novel compressively strained-layer design on a GaAs substrate with two color BLIP operation in the MWIR and LWIR bands, high detectivity, high responsivity, and high gain. Currently our efforts are centered on a dual strain P-QWIP grown on an InP substrate with a designed detective peak at 10.2 μm. Preliminary measurements indicate BLIP operation at 77 K and possibly much higher temperatures. Although extensive background work for each type of P-QWIP has been performed, more effort will be directed towards the arena of optimization and reliability in the future.

References

1. B. F. Levine, R. J. Malik, J. Walker, K. K. Choi, C. G. Bethea, D. A. Kleinman, and J. M. Vandenberg, Appl. Phys. Lett. **50**, 273 (1987).

2. L. S. Yu, S. S. Li, Appl. Phys. Lett. **59**, 1332 (1991).

3. G. Hasnain, B. F. Levine, C. G. Bethea, R. A. Logan, J. Walker, and R. J. Malik, Appl. Phys. Lett. **54**, 2515 (1989).

4. J. Y. Andersson and L. Lundqvist, J. Appl. Phys. **71**, 3600 (1992).

5. B. F. Levine, S. D. Gunapala. J. M. Kuo, S. S. Pei, and S. Hui, Appl. Phys. Lett. **59**, 1864 (1991).

6. J. Katz, Y. Zhang, and W. I . Wang, Electron. Lett. **28**, 932 (1992).

7. W. S. Hobson, A. Zussman, B. F. Levine, and J. deJong, J. Appl. Phys. **71**, 3642 (1992).

8. J. W. Matthews and A. E. Blakeslee, J. Cryst. Growth **32**, 265 (1976).

9. Landolt-B̈(o)rnstein, "Numerical Data and Functional Relationships in Science and Technology", O. Madelung, ed., Group III, **17a, 22a**, Springer-Verlag, Berlin (1986).

10. G. Ji, D. Huang, U. K. Reddy, T. S. Henderson, R. Houre, and H. Morkoç, J. Appl. Phys. **62**, 3366 (1987).

11. T. P. Pearsall, Semiconductors and Semimetals, **32**, 55 (1990).

12. H. Asai, and Y. Kawamura, Appl. Phys. Lett. **56**, 746 (1990).

13. H. Xie, J. Katz, and W. I. Wang, Appl. Phys. Lett. **59**, 3601 (1991).

14. R. T. Kuroda and E. Garmire, Infrared Phys. **34**, 153 (1993).

15. L. R. Ram-Mohan, K. H. Yoo, and R. L. Aggarwal, Phys. Rev B **38**, 6151 (1988).

16. J. M. Luttinger and W. Kohn, Phys. Rev. **97**, 869 (1956).

17. J. M. Luttinger, Phys. Rev. **102**, 1030 (1956).

18. G. L. Bir and G. E. Pikus, "Symmetry and Strain-Induced effects in Semiconductors", Wiley, New York (1974).

19. E. L. Derniak and D. G. Crowe, Optical Radiation Detectors, Wiley, New York (1984).

20. B. F. Levine, C. G. Bethea, G. Hasnain, J. Walker, and R. J. Malik, Appl. Phys. Lett. **53**, 296 (1988).

21. D. A. Scribner, M. R. Kruer, and J. M. Killiany, Proc. of the IEEE **79**, 66, (1991).

22. R. Hull, J. C. Bean, F. Cerdeira, A. T. Fiory, and J. M. Gibson, Appl. Phys. Lett. **48**, 56 (1986).

23. E. O. Kane, "Semiconductors and Semimetals", eds. R. K. Willardson and A. C. Bear, **1**, 75 (1966).

24. F. H. Pollack, "Semiconductors and Semimetals", ed. T. P. Pearsall, **32**, 17 (1990).

25. Y. C. Chang and R. B. James, Phys Rev. **B-39**, 672 (1989).

26. P. Man and D. S. Pan, Appl. Phys. Lett. **61**, 2799 (1992).

27. S. K. Chun, D. S. Pan, and K. L. Wang, Phys. Rev. **B-47**, 15638 (1993).

28. B. F. Levine, J. Appl. Phys. **74**, R1 (1993).

29. J. W. Matthews and A. E. Blakeslee, J. Cryst. Growth **27**, 118 (1974).

30. J. W. Matthews and A. E. Blakeslee, J. Cryst. Growth **29**, 273 (1975).

31. K. Hirose, T. Mizutani, and K. Nishi, J. Cryst. Growth **81**, 130 (1987).

32. H. C. Liu, Z. R. Wasilewski, and M. Buchanan, Appl. Phys. Lett. **63**, 761 (1993).

Temperature (K)	Bias (V)	Responsivity (mA/W)	Detectivity ($\frac{cm\sqrt{Hz}}{W}$)
77	4	12.10	3.92×10^{10}
	2	5.30	8.10×10^{10}
90	4	11.71	3.29×10^{10}
	2	5.34	7.60×10^{10}
100	4	13.04	1.88×10^{10}
	2	5.69	3.69×10^{10}

Table 1. Measured responsivities and detectivities as a function of applied bias and device temperature.

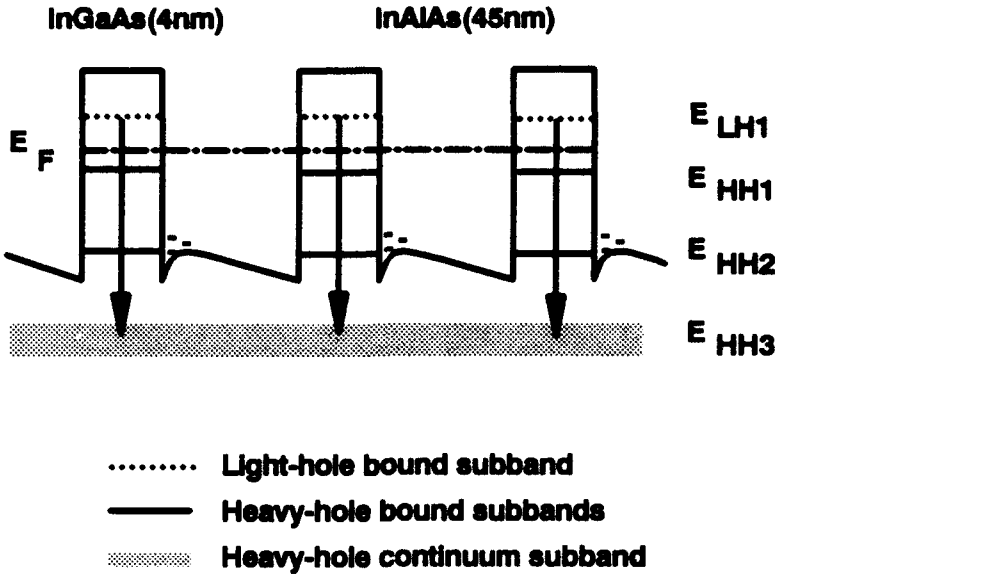

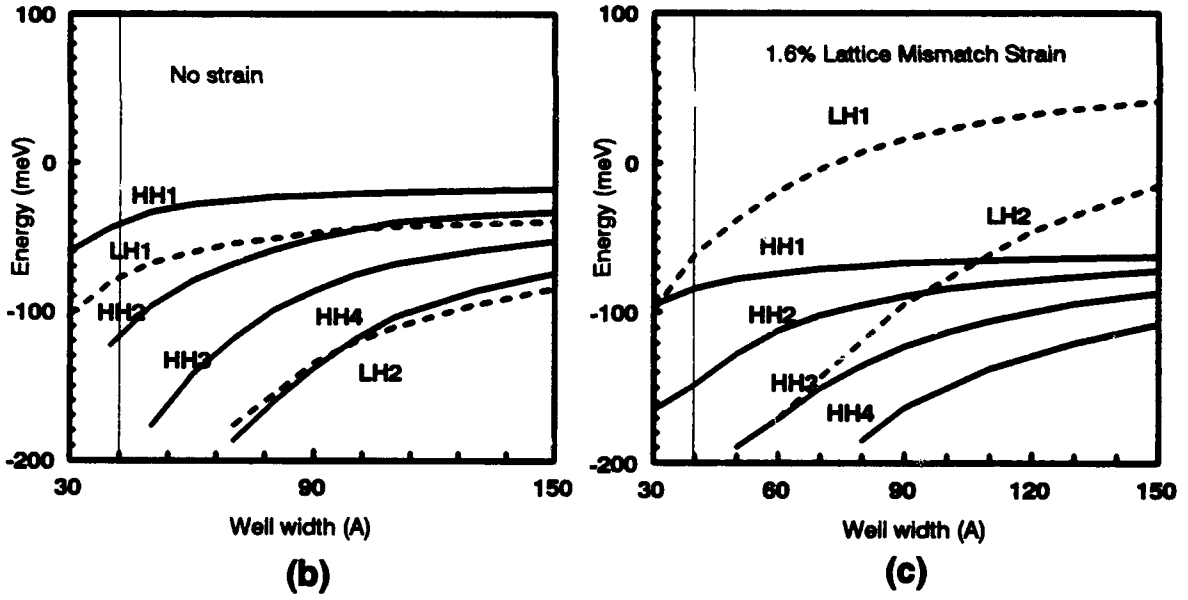

Figure 1. (a) Schematic energy band diagram for the tensile strain P-QWIP and the calculated energy levels in the quantum well for the P-QWIP (b) without and (c) with 1.6% tensile strain.

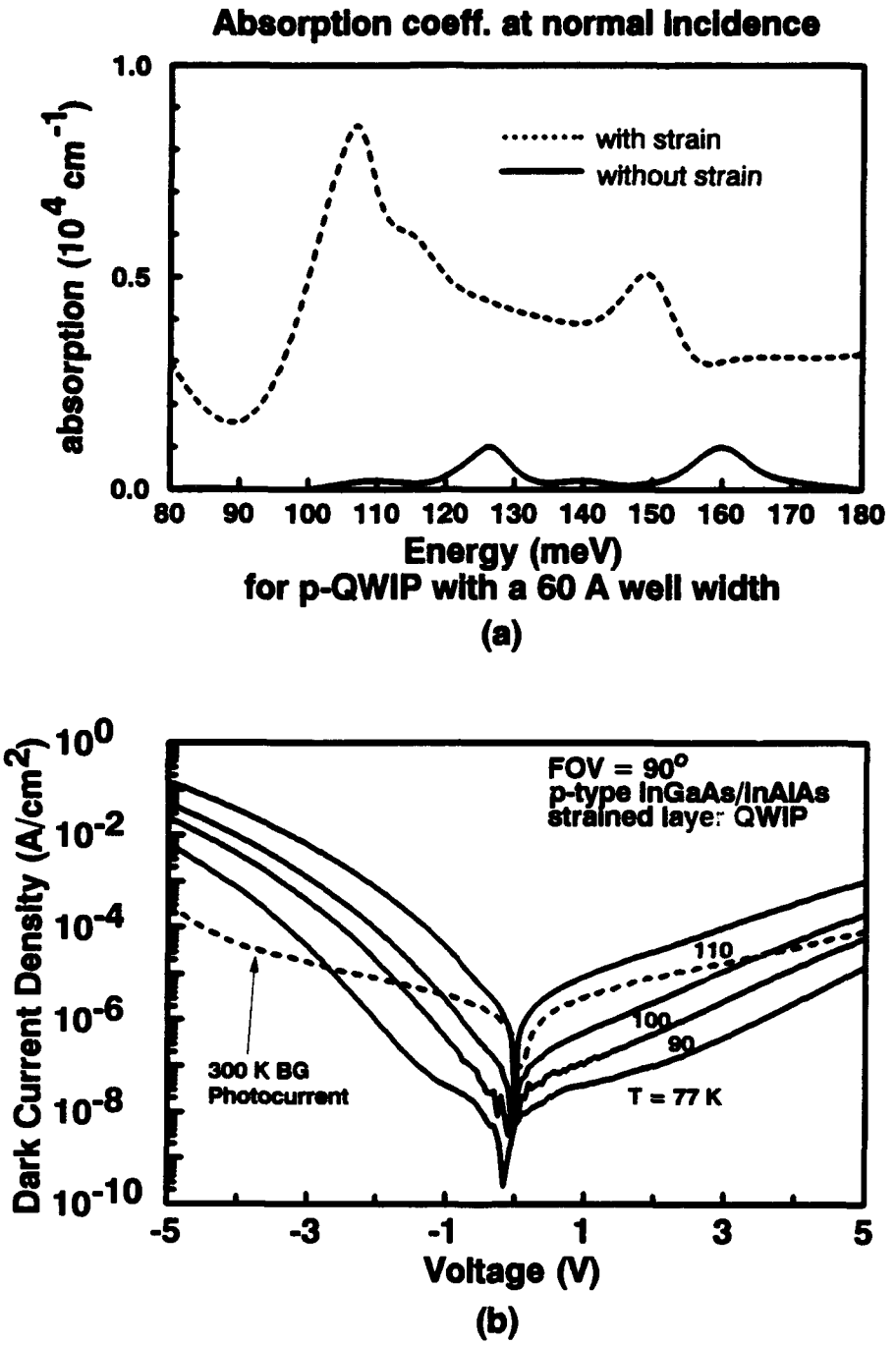

Figure 2. (a) Calculated absorption coefficient at normal incidence for a P-QWIP both with and without strain, and (b) measured dark current density and 300 K background photocurrent density.

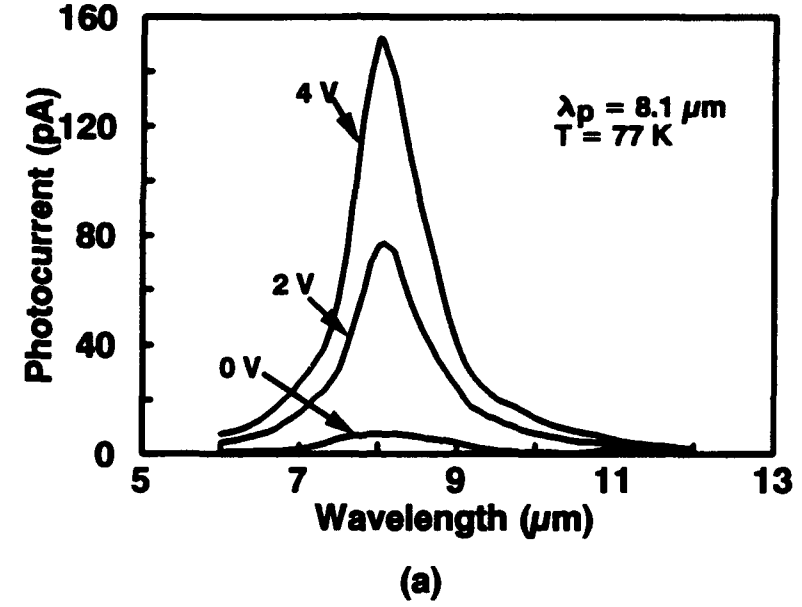

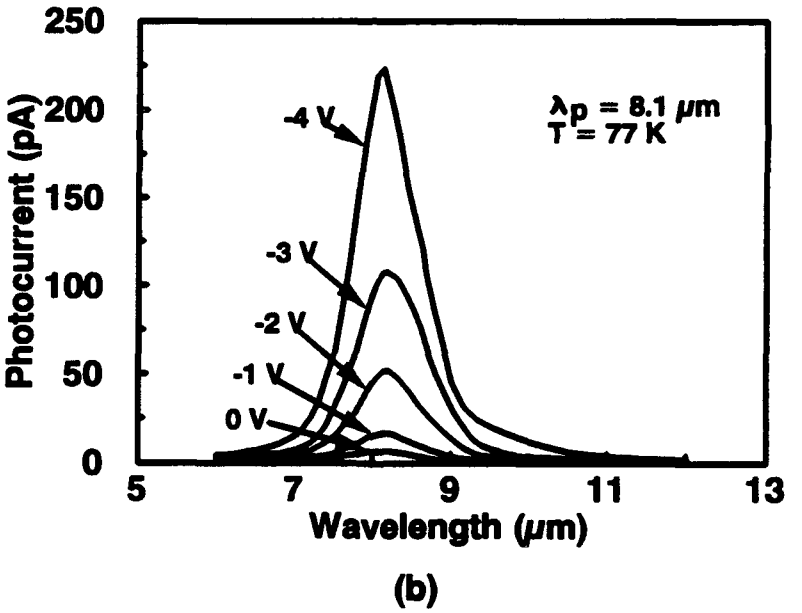

Figure 3. Measured P-QWIP photoresponse at T = 77 K for (a) forward bias and (b) reverse bias.

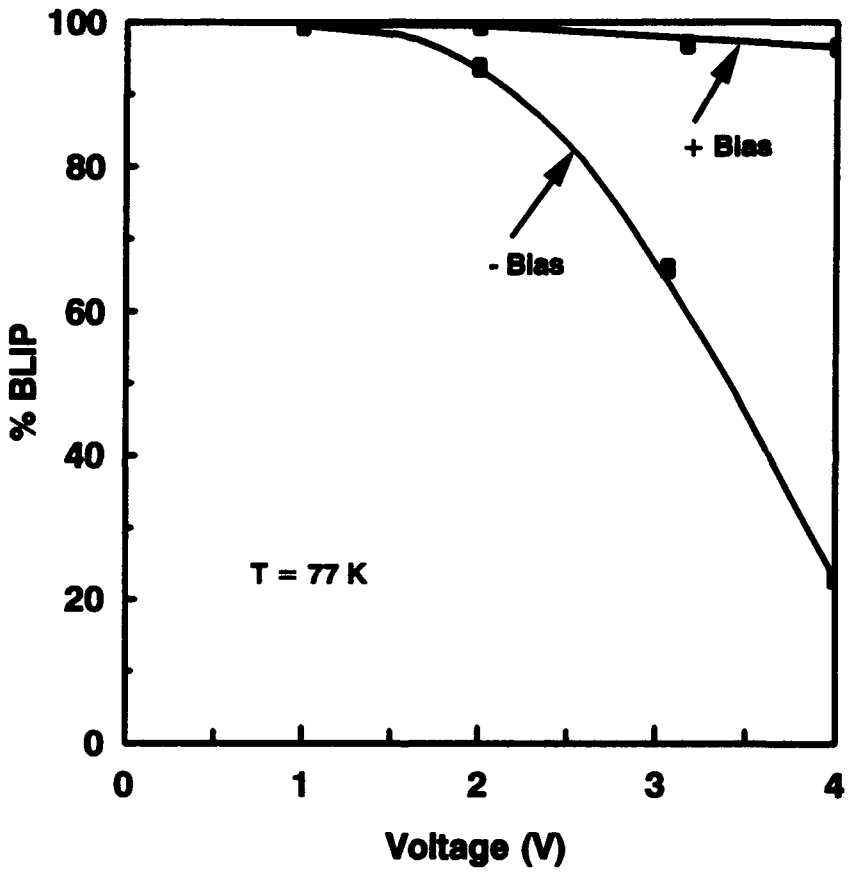

Figure 4. % BLIP for the strained-layer P-QWIP as a function of applied bias.

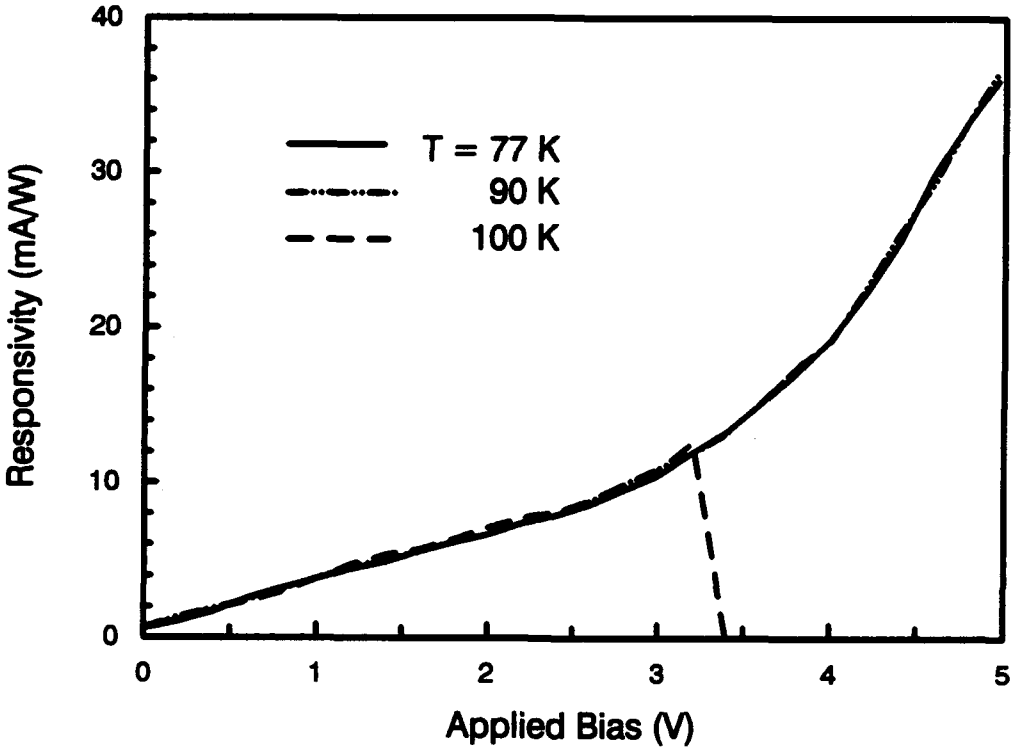

Figure 5. Responsivity as a function of bias and device temperature.

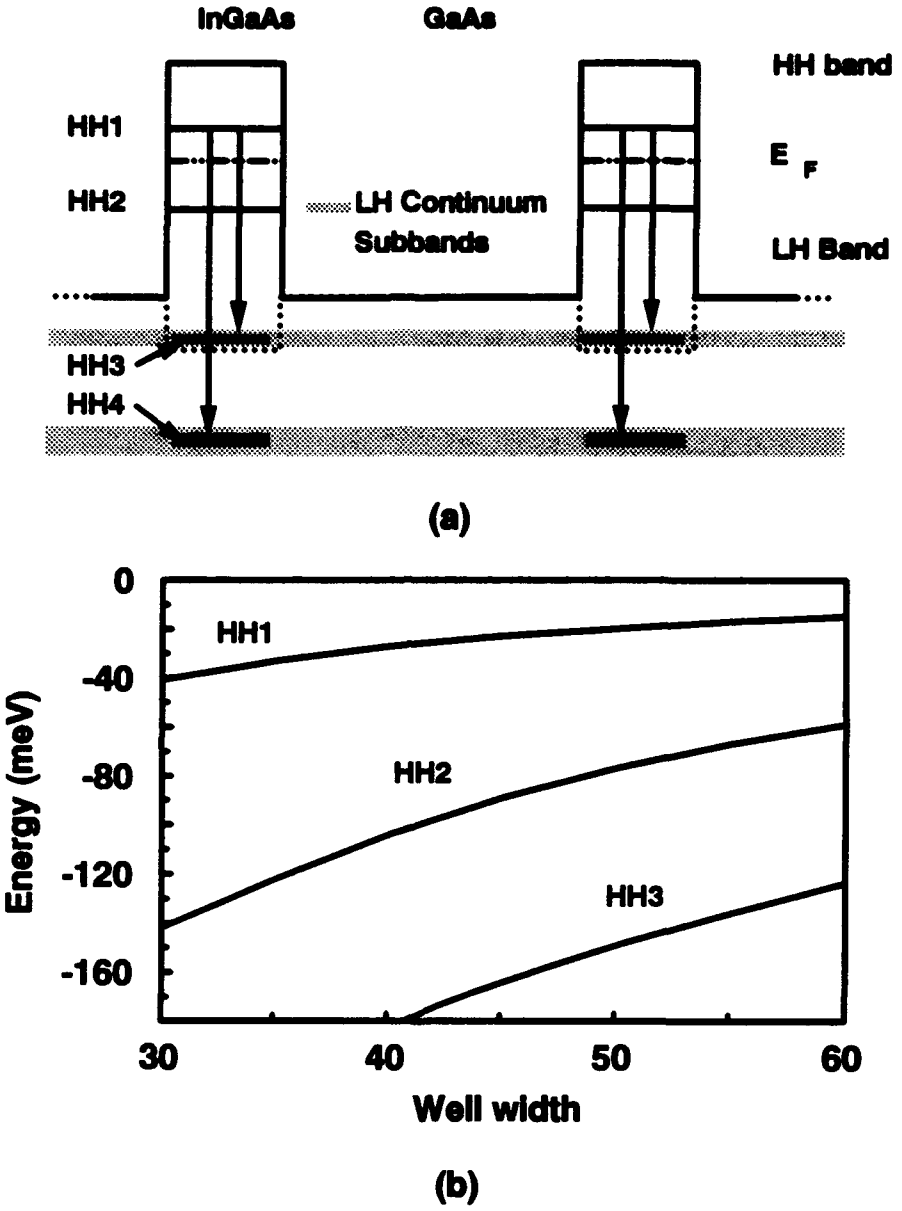

Figure 6. (a) Schematic energy band diagram for the InGaAs/GaAs compressionally strained P-QWIP and (b) the calculated energy levels in the quantum wells.

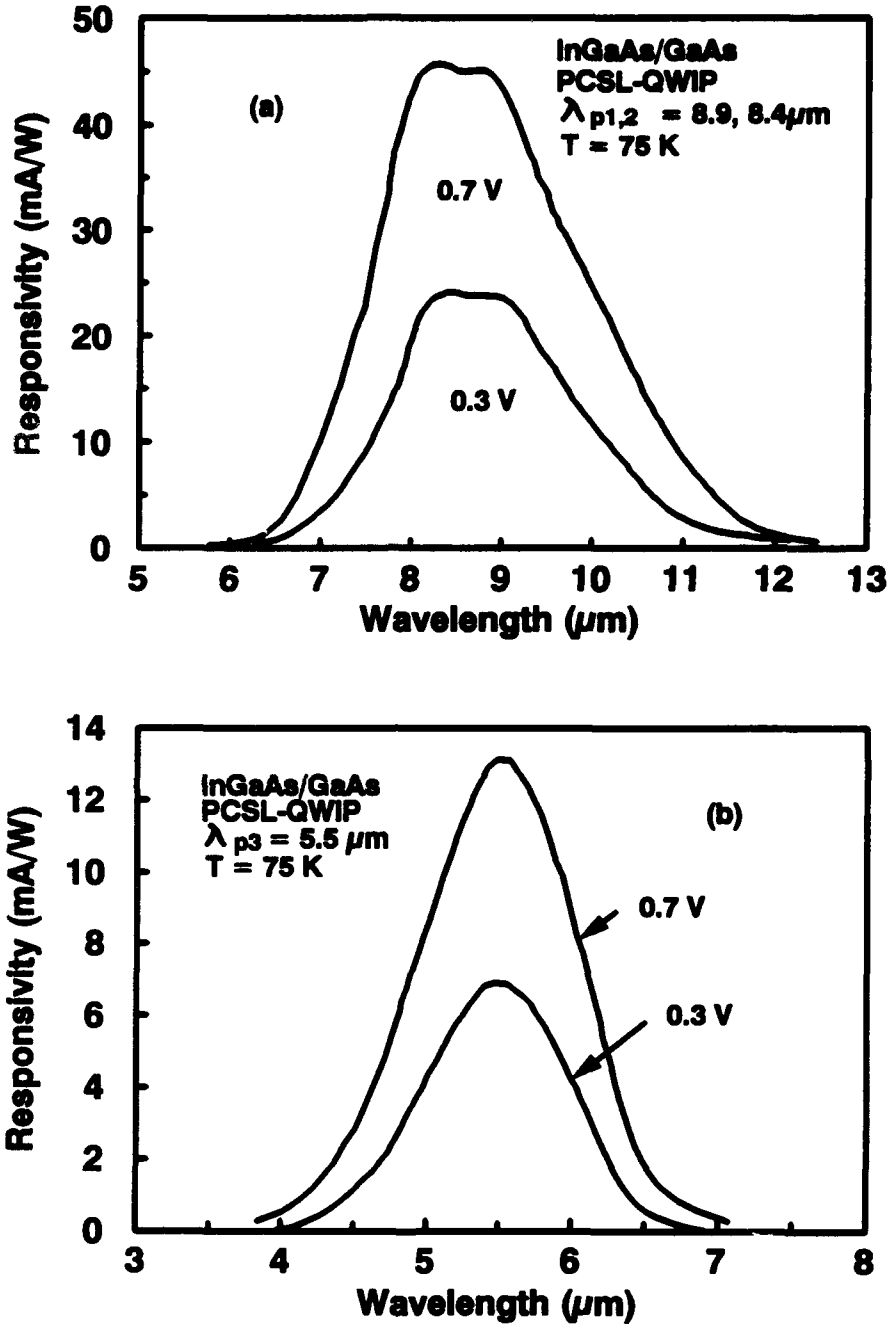

Figure 7. Measured photoresponse of the compressionally strained P-QWIP in the (a) LWIR detection band and the (b) MWIR detection band as a function of applied bias.

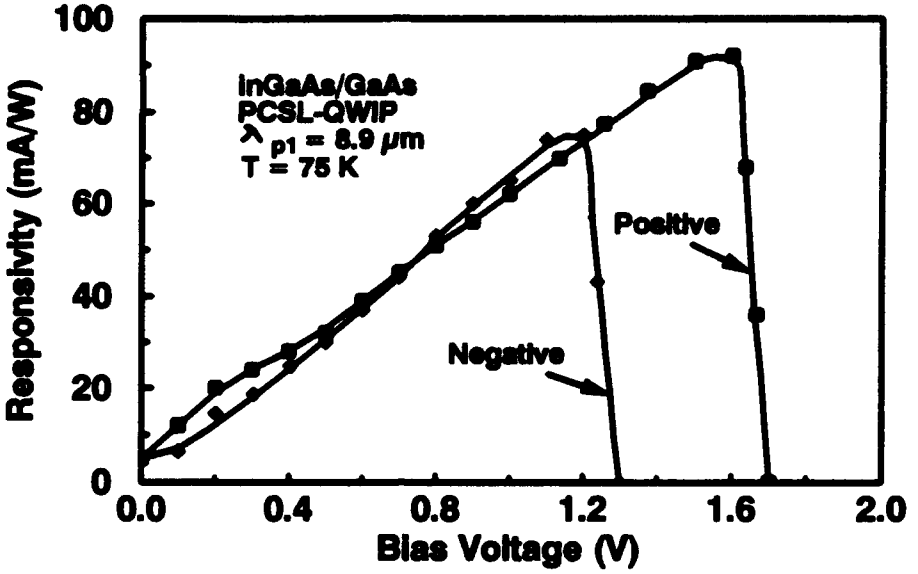

(a)

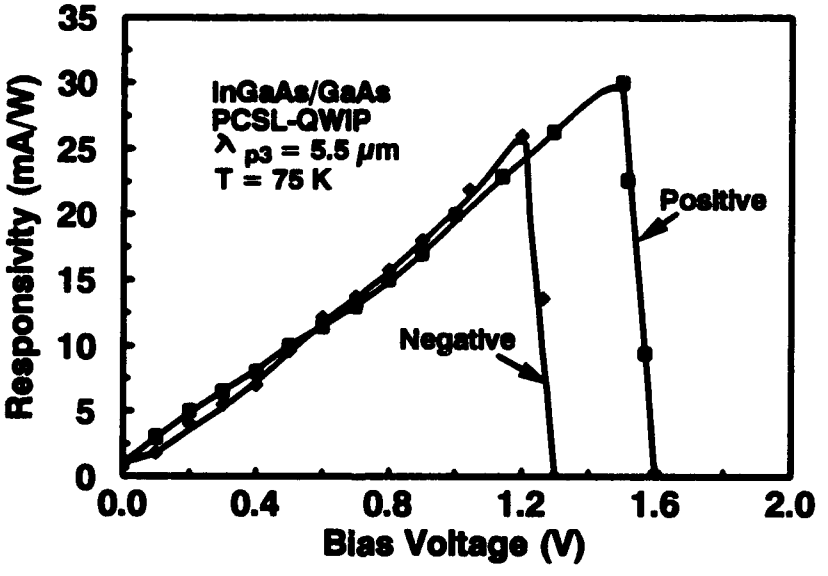

(b)

Figure 8. Measured responsivities for the compressionally strained P-QWIP as a function of applied bias for the (a) LWIR band and the (b) MWIR band.

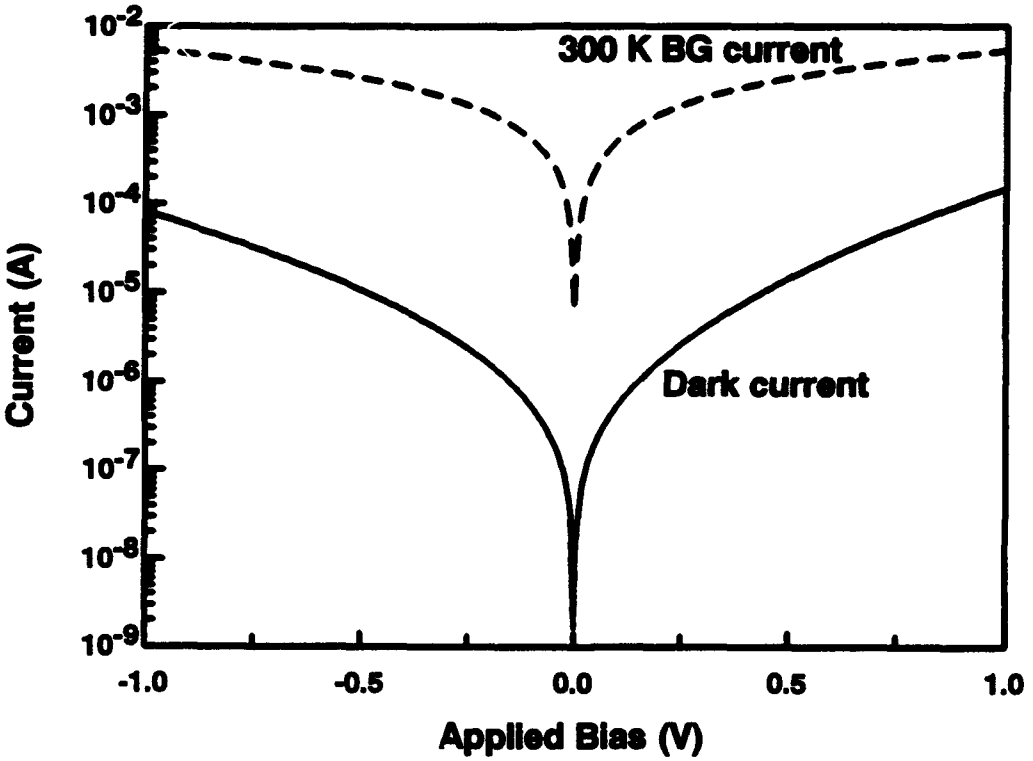

Figure 9. The measured 300 K background photocurrent and dark current at 77 K for the dual strain P-QWIP.